Biosensors and Bioelectronics 134 (2019) 29–35

Contents lists available at ScienceDirect

Biosensors and Bioelectronics

journal homepage: www.elsevier.com/locate/bios

Silver-based metal-organic gels as novel coreactant for enhancing electrochemiluminescence and its biosensing potential

Yang Li[a], Li He[a], Cheng Zhi Huang[b,**], Yuan Fang Li[a,*]

[a] Key Laboratory of Luminescent and Real-Time Analytical Chemistry (Southwest University), Ministry of Education, College of School of Chemistry and Chemical Engineering, Southwest University, Chongqing, 400715, China

[b] College of Pharmaceutical Science, Southwest University, Chongqing, 400716, China

ARTICLE INFO

Keywords:
Metal-organic gels
Electrochemiluminescence
Coreactant
Label-free biosensing

ABSTRACT

Metal-organic gels (MOGs), a kind of soft materials, were reported as a brand new category of novel solid coreactants for enhancing electrochemiluminescence (ECL) of Ru $(bpy)_3^{2+}$ and derivatives. In this work, silver-based MOGs (Ag-MOGs) prepared by a one-step mixing and heating approach were demonstrated as novel efficient solid-state coreactants which differ from the previous research on ECL coreactant nanomaterials. It was discussed that the possible enhancement mechanism was due to the amino-rich groups and the electro-catalytic effect of Ag-MOGs, endowing them promising coreactants for the enhancement of Ru $(bpy)_3^{2+}$ ECL. Interestingly, Ag-MOGs can also enhance the ECL signal of Ru $(phen)_3^{2+}$, a derivative of Ru $(bpy)_3^{2+}$ that can specifically insert into double strand DNA, further manifesting the as-prepared Ag-MOGs can be served as ideal coreactant materials. Based on the Ru $(phen)_3^{2+}$/Ag-MOGs system, a label-free signal-on ECL biosensor for detecting of target DNA was constructed to illustrate the potential application of Ag-MOGs. This research presents an effective coreactant for Ru luminophore-based ECL systems, which not only broadens the potential application of MOGs, but also offers a unique insight into the coreactant materials.

1. Introduction

Nowadays, electrochemiluminescence (ECL) has become an exceedingly superior analytical method that has appeared in various research fields due to the distinctive advantages of nearly zero background and high sensitivity (Guo et al., 2018; Hu and Xu, 2010; Liu et al., 2015). In particular, tris(2,2′-bipyridyl)ruthenium (II) (Ru $(bpy)_3^{2+}$)-coreactant system in the region of positive potentials (oxidative-reduction mechanism) has achieved overwhelming success even in commercial application, thanks to their high ECL efficiency and stable signal in aqueous solution (Miao, 2008; Valenti et al., 2016). There is no doubt that tripropylamine (TPA) as the classic coreactant can significantly enhance the ECL emission, but TPA itself is toxic, corrosive, and volatile, which will hinder its further application, especially for immunoassay and DNA detection of Ru $(bpy)_3^{2+}$(Liu et al., 2007b). Therefore, some other molecules which are more environmentally friendly employed as coreactants of Ru $(bpy)_3^{2+}$ were reported, such as 2-(dibutylamino)ethanol (DBAE) (Wu et al., 2014). In comparison with those organic molecular coreactants, nanomaterials with unique features and superior enhancements are more likely to receive the favor of researchers. For example, Wang et al. reported that the stable and enhanced ECL in the system of boron nitride quantum dots (BNQDs) and Ru $(bpy)_3^{2+}$ (Xing et al., 2018b). Zhang's group revealed that graphene quantum dots (GQDs) could be used as novel coreactant in ECL process in Ru $(bpy)_3^{2+}$/GQDs system (Qi et al., 2017b). In addition, zero-dimensional nanodots (carbon nanodots and CdSe QDs) were reported as the coreactants of Ru $(bpy)_3^{2+}$ by Pang's group and Zhu's group, respectively (Dong et al., 2015; Long et al., 2014). Notably, Cola's group developed the self-enhancing ECL by covalently linking coreactant amine-rich nitrogen-doped carbon nanodots and luminophore Ru $(bpy)_3^{2+}$ (Carrara et al., 2017). However, obtaining these reported nanomaterials inherently required complex and time-consuming procedures, utilization of organic solvent, or the possible batch to batch variation, which are unfavorable for further applications. In addition, it is not difficult to find that the currently reported coreactant nanomaterials are mainly concentrated in zero-dimensional nanodots, and other types of materials have rarely been reported as coreactants. In these regards, it is very promising to develop a new category of nanomaterial as novel coreactant candidates using a rapid, facile and green route.

* Corresponding author.
** Corresponding author.
E-mail addresses: chengzhi@swu.edu.cn (C.Z. Huang), liyf@swu.edu.cn (Y.F. Li).

https://doi.org/10.1016/j.bios.2019.03.058
Received 14 January 2019; Received in revised form 7 March 2019; Accepted 26 March 2019
Available online 29 March 2019

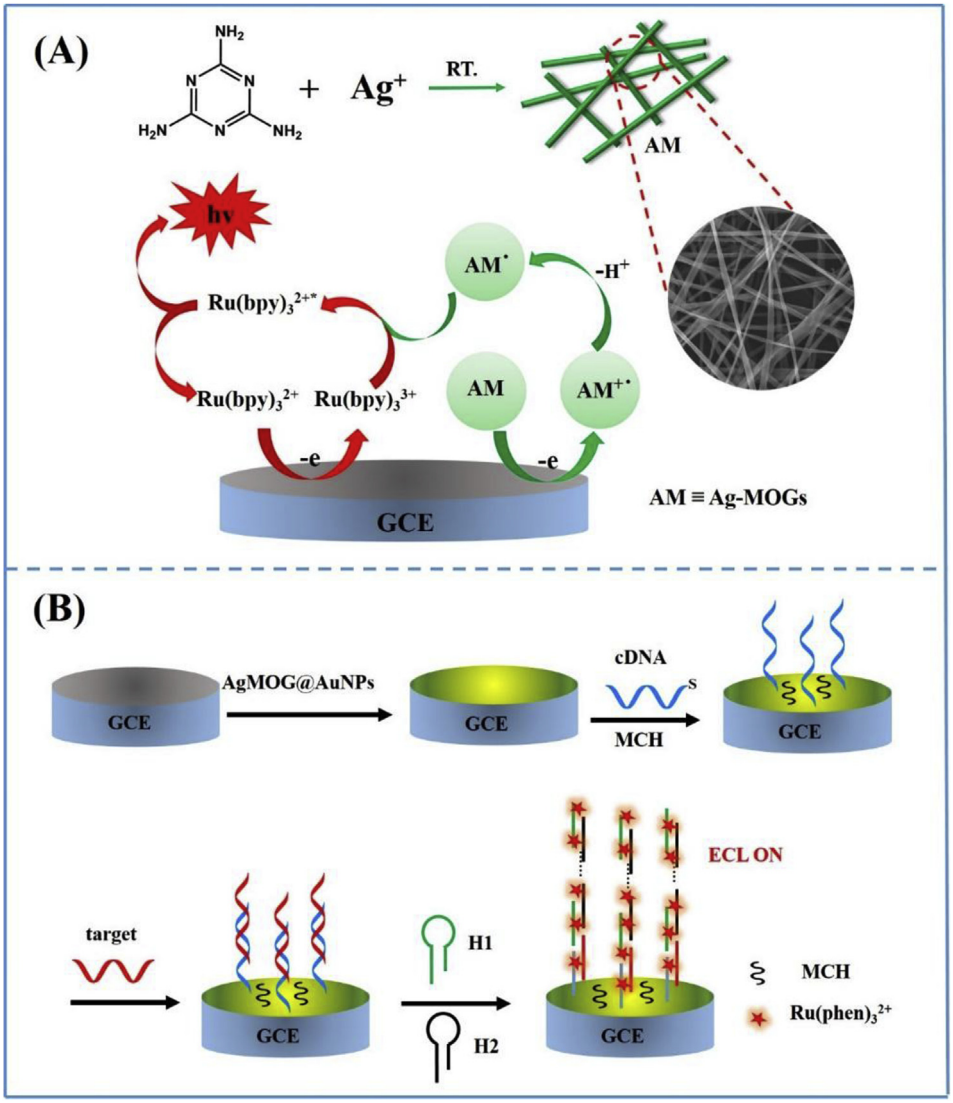

Scheme 1. (A) The preparation of Ag-MOGs and the proposed possible mechanism for enhancing ECL of Ru $(bpy)_3^{2+}$. (B) Illustration of the HCR-based label-free biosensor for detecting target DNA.

In these years, metal-organic gels (MOGs), the smart coordination polymers soft materials, are appearing as alternative candidates to well-known metal-organic frameworks (Vallejo-Sánchez et al., 2017). This kind of gels has gradually become new stars in the field of sensing (Peng et al., 2017; Shih et al., 2017; Tang et al., 2018), adsorption (Jayaramulu et al., 2017), catalysis (Karan et al., 2017; Tu et al., 2007), crystal phase transition (Qi et al., 2017c), or antibacterial (Qin et al., 2015; Thakur et al., 2018). Recently, our group reported terbium-based organic gels can be used as the novel ECL emitters (Li et al., 2018), which motivated us to explore whether MOG materials can also be used as ECL coreactants. As we all know, on the one hand, various auxiliary moieties such as amide/amine hydrogen-bonding motifs and long alkyl chains have been introduced into coordination polymers to assist the gelation process (Falcone and Kraatz, 2018; Sun et al., 2018; Zhang and Su, 2013). On the other hand, previous works indicated that a wide range of amino compounds have great potential as the "oxidative-reduction" coreactants in ECL field (Fähnrich et al., 2001; Kitte et al., 2016; Li et al., 2017). Thus, MOGs materials have great potential to be revolutionary ECL coreactants due to their extremely facile synthetic method and the rich potential amino functional groups. Keeping in mind that there are no related report, it is an exciting chance to prepare novel MOGs with a facile way and gather efficient ECL enhancement performance.

Melamine (1,3,5-triazine-2,4,6-triamine), which has a number of amino-groups, possesses unusual coordination ability with metal ions and has been used to synthesize various functional materials (Bai et al., 2018; Fei et al., 2013). MOGs materials obtained by employing melamine as the ligand can combine the advantages of simple synthesis and retain the rich amino sites. Thus, melamine may be applied as a good candidate of complexing agent to acquire ECL coreactant materials.

With these in mind, the silver-based metal-organic gels (Ag-MOGs) were reported as novel solid coreactants for enhancing ECL of Ru $(bpy)_3^{2+}$. Ag-MOGs were synthesized via a rapid one-step mixing and heating route which only required to mix amino-rich melamine and Ag^+ for self-assembly. Intriguingly, when Ag-MOGs were introduced as ECL coreactants, the Ru $(bpy)_3^{2+}$ exhibited a significant around 40-fold enhancement ECL intensity and stability in the presence of Ag-MOGs. Further, Ag-MOGs was found to enhance the ECL of Ru $(phen)_3^{2+}$ (see Fig. S1 for the structure), the derivative of Ru $(bpy)_3^{2+}$, as well. The potential application of Ag-MOGs as the coreactant was illustrated by detecting target DNA. This work has offered an extremely new coreactant material that is completely different from the currently reported coreactant nanomaterials, and is highly likely to be widely used due to the rapid green synthesis and excellent ECL enhancement performance.

2. Experimental section

Reagents and characterized instruments were presented in Supplementary Data file.

2.1. Preparation of Ag-MOGs

Ag-MOGs was obtained through a facile one-step mixing and heating method. In a typical preparation of Ag-MOGs, 10 μL of 2.5 M $AgNO_3$ aqueous solution was added to 2 mL of 25 mM melamine aqueous solution, the solution was heated at 80 °C for about 30 s to obtain the clear solution, then taken out and slowly cooled at room temperature. Finally, the opaque white metal-organic gels were observed and evaluated based on the tube inversion test (Fig. S2). It's interesting that only Ag^+ can specifically form hydrogel with melamine, and other metals do not form gels with melamine (Fig. S3). For further use, the Ag-MOGs was dried by freeze-drying treatment to obtain the Ag-MOGs powder.

2.2. Fabrication of Ag-MOGs modified GCE

All GCE (Φ = 3 mm) used during this experiments were first polished with 0.3 and 0.05 μm Al_2O_3 powder, followed by successive sonication with ethanol and distilled water, then the cleaned electrodes were allowed to dry in a N_2 atmosphere. Subsequently, 5 μL of 2 mg/mL of Ag-MOGs was dropped to GCE surface and dried at room temperature. Afterwards, the Ag-MOGs/GCE was applied for further electrochemical measurements.

2.3. Construction of $Ru(phen)_3^{2+}$/Ag-MOGs biosensing platform

The construction process was sketched as scheme 1B. All the hairpin DNA were annealed by heating at 95 °C for 3 min and slowly cooling to 25 °C. The proposed ECL signal-on biosensor of detecting target DNA (tDNA) employs DNA sequence related to urinary tract infections as the model DNA (Chen et al., 2012). The label-free ECL biosensor based on HCR was constructed as follows: 5 μL of 2 mg/mL of Ag-MOGs and AuNPs were dropped on the GCE, respectively. Then, 5 μL of 2 μM thiolated capture DNA (cDNA) was dripped onto the modified electrode and incubated overnight, then 1 mM 6-mercapto-1-hexanol (MCH) was used to blocked non-specific sites for 2 h. Next, 8 μL of tDNA was added to the electrode and incubated for 2 h. Subsequently, 5 μL of hairpin DNA H1 and H2 (1 mM each) was dropped to the prepared electrodes and incubated for 4 h. Afterwards, 8 μL of 2 mM of Ru $(phen)_3^{2+}$ was dropped on the electrode and incubated for 5 h. The electrode was rinsed with buffer solution after each step. At last, ECL intensity of the resulting modified electrodes were tested from 0 to 1.3 V (versus Ag/AgCl).

3. Results and discussion

3.1. Characterization of Ag-MOGs

The morphological property of this facile one-step synthetic gel was investigated by scanning electron microscope (SEM). The SEM image (Fig. 1A) revealed the fibrous nature of the obtained Ag-MOGs; the three-dimensional nanofibers have a diameters of about 250 nm and can reach a length of several micrometers. Next, the viscoelastic (gel) property of this gel was characterized by rheology investigation. Fig. 1B showed the variation of storage modulus (G′) and loss modulus (G″) relative to applied frequency for Ag-MOGs. G′ and G″ are almost independent frequencies and G′ was greater than G″ at any given point, indicating the true gel-like nature of Ag-MOGs which was consistent with the visually observable inverted phenomenon (Fig. 1B, insert). To explore the coordination of melamine and Ag^+, Fourier transform infrared (FTIR) spectrometer and ^1H nuclear magnetic resonance (^1H NMR) spectra were carried out. As shown in Fig. 1C, the vibration frequencies of the semicircle stretching of triazine ring at 1465 to 1436 cm^{-1} shifted to 1440 to 1393 cm^{-1}, indicating that the lone pair of electrons of a nitrogen atom donated to Ag^+ (Bairi et al., 2011). The ^1H NMR spectra of melamine and Ag-MOGs (Fig. 1D) showed that the coordination of Ag^+ and melamine caused the chemical shifts of melamine in the range of 2.0–8.0 ppm to move slightly upfield with a shift of 0.5 ppm, which presumably ascribed to that aromatic protons experienced a shielding effect by the π cloud of the neighboring aromatic moiety through π-π or C-H … π interations (Majumder and Dastidar, 2016). These results manifested the coordination of melamine and Ag^+, and the presence of π-π stacking.

X-ray diffraction analysis (XRD) and X-ray photoelectron spectroscopy (XPS) were surveyed to further analyze the chemical and physical structure of Ag-MOGs. The XRD of $AgNO_3$, melamine and formed Ag-MOGs were compared, as shown in Fig. 2A. The distinct XRD patterns of the components and Ag-MOGs indicated the different crystalline structures. Especially for Ag-MOGs, the amorphous nature of this material was confirmed by the selected area electron diffraction (SAED) investigation (Fig. S4) (Dhara et al., 2014). Further, the surface chemical compositions of the Ag-MOGs was analyzed by XPS. As shown in Fig. 2B, the main strong carbon (C 1s), nitrogen (N 1s) and silver (Ag 3d) signal peaks are presented in the XPS analysis which was in agreement with the SEM-EDS results (Fig. S5), consequently demonstrating the existence of a large amount of these elements.

3.2. Ag-MOGs as the efficient coreactants of $Ru(bpy)_3^{2+}$

As the “war horse” in ECL systems, Ru $(bpy)_3^{2+}$, generally follows the coreactant ECL pathway based on a reaction cascade between the sacrificial coreactant species and the luminophore (Sentic et al., 2014). With the ever-increasing development of nanotechnology, novel ECL coreactant nanomaterials are in great demand. In this article, we developed the Ru $(bpy)_3^{2+}$/Ag-MOGs system, in which Ag-MOGs was the coreactant and Ru $(bpy)_3^{2+}$ was the emitter. As Fig. 3 shown, pure 1 mg/mL Ru $(bpy)_3^{2+}$ only had an extremely weak ECL intensity (about 70 a. u), which is consistent with previous reported that individual Ru $(bpy)_3^{2+}$ can emit weak light obeying the annihilation pathway (Richter, 2004). But individual Ag-MOGs exhibited no ECL intensity, indicating that Ag-MOGs can't perform as ECL emitters in this system. Strikingly, in the presence of Ag-MOGs, an obvious enhanced ECL (about 40-fold enhancement) of Ru $(bpy)_3^{2+}$ was observed. These results suggested that the ECL emission of Ru $(bpy)_3^{2+}$/Ag-MOGs system was derived from Ru $(bpy)_3^{2+}$ and enhanced by Ag-MOGs.

Further, the influence of Ag-MOGs concentration and pH were also investigated. As shown in Fig. S6A, the ECL intensity increased sharply correspondingly as the pH increased from 5.5 to 7.5, indicating that deprotonation is a key step in the ECL process (Qi et al., 2017a). But the ECL intensity decreased at higher pH, which may be due to that the over-alkali conditions may damage the MOGs materials and do not allow the materials to be well immobilized on the electrode surface. Similarly, the ECL intensity increased with the concentration of Ag-MOGs in a range of 0.25 mg/mL to 2 mg/mL due to that more coreactants will participate in the ECL process (Fig. S6B). But the ECL intensity will decreased if further increase of the concentration of Ag-MOGs, which could attribute to the side reactions at high-concentrations (Liu et al., 2007a).

To further shed light on the mechanism of Ag-MOGs as coreactants, UV-vis absorbance, cyclic voltammogram (CV) measurements and corresponding ECL measurements were performed. As can be seen in Fig. S7, in the range of 220–650 nm, the UV-vis spectra of mixture of Ru $(bpy)_3^{2+}$/Ag-MOGs was nearly equal to the sum of the separated Ru $(bpy)_3^{2+}$ and Ag-MOGs. This revealed that there was no new species formed in the mixture of Ag-MOGs and Ru $(bpy)_3^{2+}$ and the ECL emission would be attributed to the reaction between the substances obtained by the electrochemical reaction of Ru $(bpy)_3^{2+}$ and Ag-MOGs.

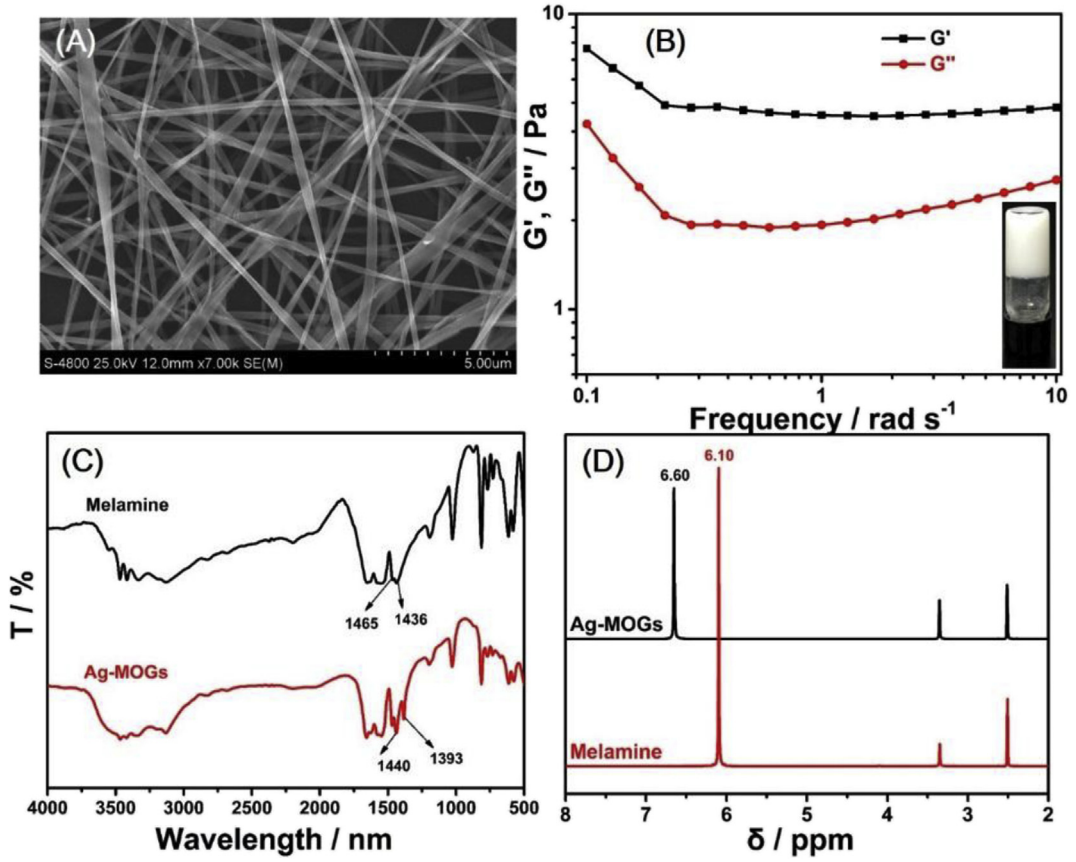

Fig. 1. (A) SEM characterization of Ag-MOGs. (B) Plot of storage modulus (G′) and loss modulus (G″) with frequency for Ag-MOGs. The insert: the photograph of inverted Ag-MOGs. (C) FTIR spectra of melamine and Ag-MOGs. (D) ^{1}H NMR spectrum of Ag-MOGs and melamine.

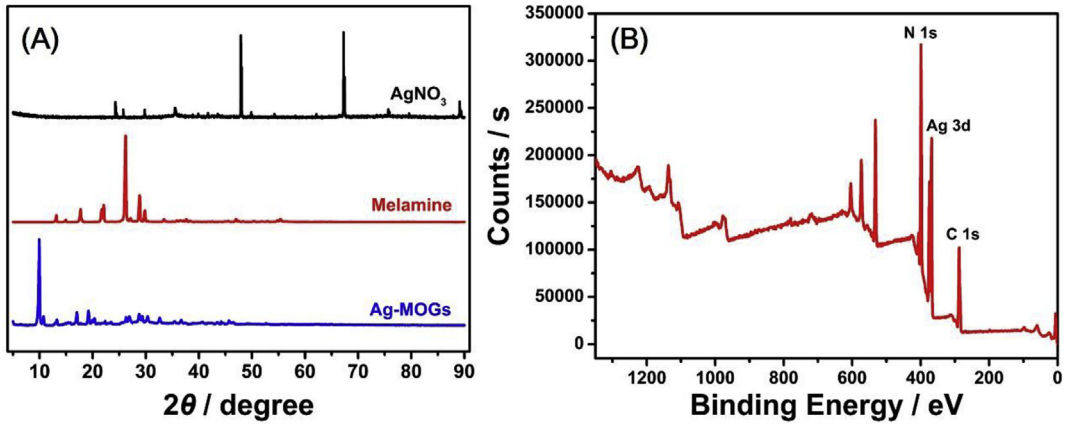

Fig. 2. (A) XRD pattern of $AgNO_3$, melamine and Ag-MOGs. (B) XPS survey of Ag-MOGs.

Subsequently, we compared the ECL-potential curves of Ru $(bpy)_3^{2+}$, Ag-MOGs, and Ru $(bpy)_3^{2+}$/Ag-MOGs, Ru $(bpy)_3^{2+}$/Ag^+, Ru $(bpy)_3^{2+}$/melamine systems, respectively. As shown in Fig. 4A and Fig. 4B, the ECL emission of Ru $(bpy)_3^{2+}$ can be enhanced in the presence of Ag-MOGs or melamine, indicating that the enhancement of Ru $(bpy)_3^{2+}$ by Ag-MOGs may derive from the ligand (melamine). In order to verify our speculation, we carried out the CV experiments. Fig. 4C shows the CV curves of 1 mM Ru $(bpy)_3^{2+}$ on the 5 μL of 2 mg/mL Ag-MOGs modified GCE surface in PBS, respectively. In the absence of Ag-MOGs, only the reversible oxidation peak of Ru $(bpy)_3^{2+}$ was observed; and the bare Ag-MOGs shows a oxidation peak at about 0.6 V. However, upon addition of Ag-MOGs, the intensity of the oxidation peak of Ru $(bpy)_3^{2+}$ increased. The performance may suggest the catalytic effect of Ag-MOGs on the Ru $(bpy)_3^{2+}$ oxidation (Jin et al., 2010; Miao et al., 2002). In addition, the oxidation peak of Ag-MOGs moves to a lower potential (about +0.5 V), indicating that Ru $(bpy)_3^{2+}$ can also promote the oxidation of Ag-MOGs, which is beneficial for the ECL process. These results indicated the synergistic effect between Ag-MOGs and Ru $(bpy)_3^{2+}$, which ensured the efficient ECL processes. The CV curves of Ru $(bpy)_3^{2+}$, melamine, and Ru $(bpy)_3^{2+}$/melamine system in Fig. 4D showed that melamine remarkably increased the oxidation and reduction current, manifesting a Ag-MOGs catalytic effect on Ru $(bpy)_3^{2+}$ oxidation. These results above demonstrated that Ag-MOGs can be used for enhancing ECL of Ru $(bpy)_3^{2+}$, and the enhancement source is mainly from the ligand of Ag-MOGs. However, the effect of Ag-MOGs for enhancing ECL is significantly better than that of melamine, which

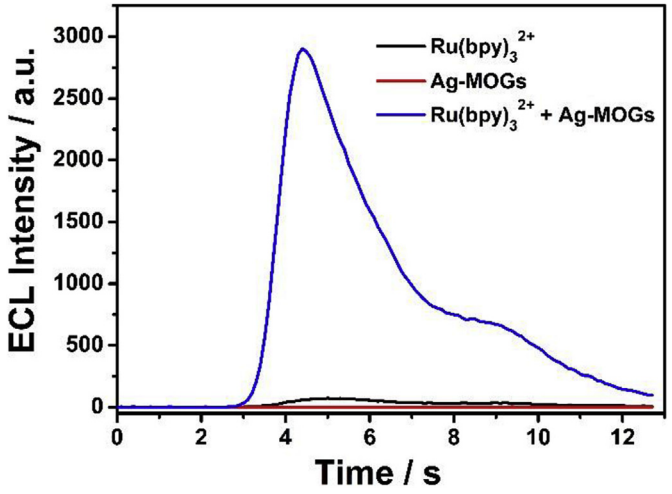

Fig. 3. ECL response of 1 mM Ru $(bpy)_3^{2+}$, 2 mg/mL Ag-MOGs, and 1 mM Ru $(bpy)_3^{2+}$ in the presence of 2 mg/mL Ag-MOGs, respectively.

may be due to that the presence of richer amino components in the gel after the coordination of melamine and Ag^+.

From the observed behavior above, a possible mechanism was proposed, sketched as scheme 1A. The higher ECL signals caused by Ag-MOGs may derive from the catalytic oxidation between the amino group of Ag-MOGs and Ru $(bpy)_3^{2+}$. Briefly, the amino group of Ag-MOGs and Ru $(bpy)_3^{2+}$ were firstly electrochemically oxidized to Ag-MOGs ($-NH_2^{+\cdot}$) and Ru $(bpy)_3^{3+}$ on the electrode surface, respectively. Then, the Ag-MOGs ($-NH_2^{+\cdot}$) experienced a deprotonation process and generated the reducing intermediate Ag-MOGs ($-NH^{\cdot}$). Finally, the reduced Ag-MOGs ($-NH^{\cdot}$) reacted with oxidized Ru $(bpy)_3^{3+}$ to form the excited state Ru $(bpy)_3^{2+*}$ which can produce ECL emission when it back to the ground state (Xing et al., 2018a). Thus this mechanism was similar to that proposed for the Ru $(bpy)_3^{2+}$/TPA ECL system (Richter, 2004) and summarized as follows:

$$Ru(bpy)_3^{2+} - e \rightarrow Ru(bpy)_3^{3+} \quad (1)$$

$$Ag\text{-}MOGs(-NH_2) - e \rightarrow Ag\text{-}MOGs(-NH_2^{+\cdot}) \quad (2)$$

$$Ag\text{-}MOGs(-NH_2^{+\cdot}) - H^+ \rightarrow Ag\text{-}MOGs(-NH^{\cdot}) \quad (3)$$

$$Ag\text{-}MOGs(-NH^{\cdot}) + Ru(bpy)_3^{3+} \rightarrow Ru(bpy)_3^{2+*} + products \quad (4)$$

$$Ru(bpy)_3^{2+*} \rightarrow Ru(bpy)_3^{2+} + h\upsilon \quad (5)$$

3.3. Application of Ag-MOGs as solid-state coreactants in nucleic acid detection

Although Ru $(bpy)_3^{2+}$ has many advantages in the ECL system, Ru $(phen)_3^{2+}$, an analog of Ru $(bpy)_3^{2+}$, which can highly affinity embedded in the groove structure of double strand DNA (ds-DNA), was an efficient ECL signal molecule and more advantageous than Ru $(bpy)_3^{2+}$ in the nucleic acid detection (Peng et al., 2018; Wang et al., 2018). To our surprise, the as-prepared Ag-MOGs also can efficiently enhance the ECL signal of Ru $(phen)_3^{2+}$ in neutral conditions, as shown in Fig. S8, suggesting that Ag-MOGs can be employed as the coreactants of Ru $(phen)_3^{2+}$.

To demonstrate the potential application of Ag-MOGs, a "signal-on" HCR-based biosensor was constructed for the detection of tDNA. Firstly, the feasibility of HCR amplification was examined by native polyacrylamide gel electrophoresis (PAGE) analysis. As seen in Fig. S9, since both capture DNA (cDNA) and target DNA (tDNA) are short single-strand DNA, no significant bands are visible on the electrophoresis, but the mixture of cDNA and tDNA (Lane 3) showed distinct bright band, demonstrating that they can hybridize to form double-stranded DNA. Compared to Lane 1, the weak and longer band in Lane 4 indicated

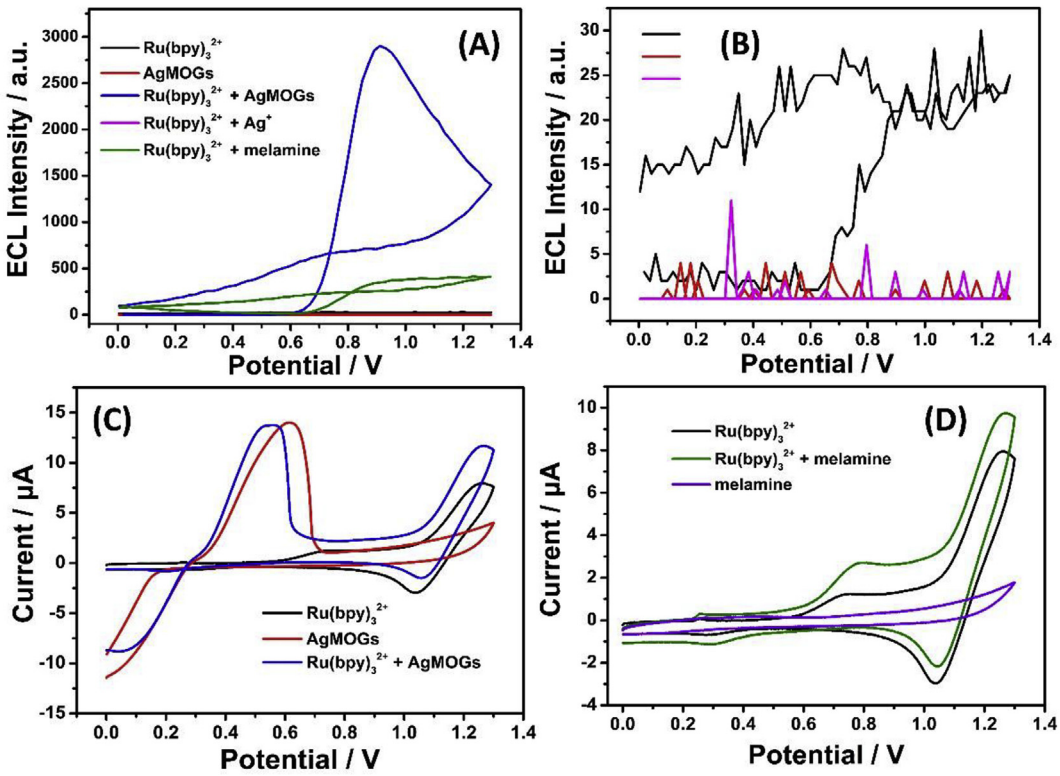

Fig. 4. (A–B) ECL-potential curves of individual Ag-MOGs, individual Ru $(bpy)_3^{2+}$, Ru $(bpy)_3^{2+}$/Ag-MOGs system, Ru $(bpy)_3^{2+}$/Ag^+ system, and Ru $(bpy)_3^{2+}$/melamine systems. (C) CV curves of Ru $(bpy)_3^{2+}$, AgMOGs, and Ru $(bpy)_3^{2+}$/Ag-MOGs system, respectively. (D) Cyclic voltammetry curves of Ru $(bpy)_3^{2+}$, melamine, and Ru $(bpy)_3^{2+}$/melamine systems, respectively.

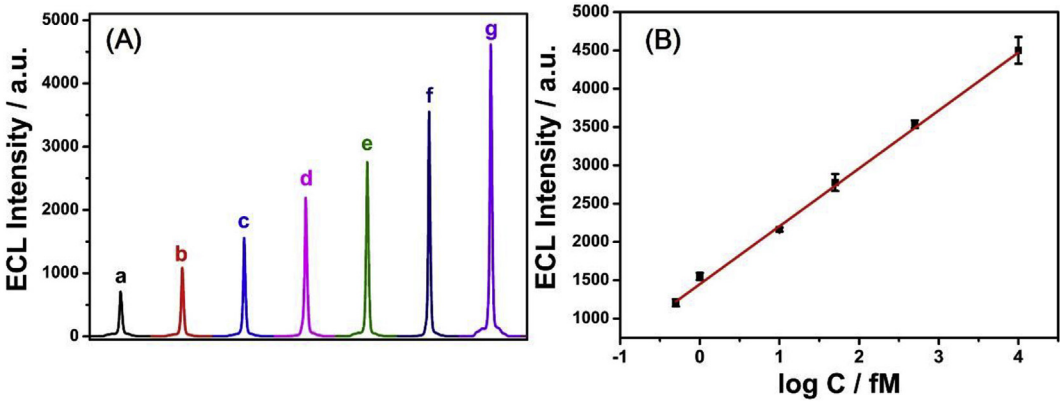

Fig. 5. (A) ECL response of constructed biosensor to various concentration of target DNA (a–g: 0, 10, 50, 100, 250, 1000, 2500 fM) (B) The resulting calibration plot, $R^2 = 0.993$.

hairpin H1 can hybridize with tDNA. In addition, the mixture of H1, H2 and tDNA (Lane 5) possessed the lowest migration rate, indicating that the system behaved as expected: half of the sequence in tDNA react with cDNA to form double strand, and the other half of the sequence opens hairpin H1, followed by a subsequent HCR reaction. That is, tDNA was used as the "link-DNA" to link cDNA and the mixture of H1 and H2.

The fabrication procedure was displayed as Scheme 1B, the detailed nucleic acid sequences are placed in Table S1. In short, Ag-MOGs and gold nanoparticle (AuNPs) were immobilized onto GCE first, then the thiolated modified capture DNA (cDNA) was introduced to the surface of GCE via Au-S bond. In the presence of the tDNA, each tDNA molecule has the capability to trigger the HCR between hairpin H1 and H2 to form an extended dsDNA polymer. Finally, a large number of Ru $(phen)_3^{2+}$ were intercalated into the grooves of the dsDNA polymers. The result is that the ECL response of the biosensor correlated with different concentration of the tDNA. The more tDNAs were introduced, the more double strand DNAs are generated, the more Ru $(phen)_3^{2+}$ were embedded into the double strand DNAs, and the resulting ECL signal will be stronger.

The designed ECL biosensor based on Ru $(phen)_3^{2+}$/Ag-MOGs was used to quantitative measurement of target DNA. In Fig. 5A, the ECL intensity (I) increased accordingly with the increasing concentrations of target DNA. The ECL intensity was linearly with the logarithm of concentration of target DNA ($\log c_{target}$) in the range from 10 fM to 2.5 pM. The linear regression equation was $I = 1449.3 + 755.9 \log c_{target}$ with a limit detection of 3.2 fM (S/N = 3), and the correlation coefficient was $R^2 = 0.993$ (Fig. 5B). Compared to previously reported nucleic acid detection systems, our Ru $(phen)_3^{2+}$/Ag-MOGs system displayed comparable or even better sensitivity (Table S2). In addition, we examined the selectivity because the specificity of a sensor play an important role in analytical testing. The selectivity of biosensors was evaluated by using complementary, three-base mismatched and non-cDNA sequence as trigger DNA, respectively (Fig. S10). In line with our expectations, the ECL signal did not show an obvious change, which means that the Ag-MOGs biosensor could provide a selective platform for quantitative detection of target DNA.

4. Conclusions

In summary, the unrevealed ECL enhancement property of Ag-MOGs was investigated by employing Ru $(bpy)_3^{2+}$ as model ECL luminophore. Compared with bare Ru $(bpy)_3^{2+}$, a 40-fold enhanced ECL was obtained thanks to the synergistic effect of Ag-MOGs and Ru $(bpy)_3^{2+}$. Further, a signal-on biosensor based on the label-free HCR amplification was constructed to detect target DNA with desirable stability and selectivity. Notably, Ag-MOGs as the efficient coreactants has some unique advantages compared with previous reports: (i) extremely green and mild synthetic method without complex post-processing; (ii) a new class of solid-state coreatants that differ from more reported nanodots; (iii) significant ECL enhancement of Ru $(bpy)_3^{2+}$ and its analogues in neutral conditions. This work pioneered the utilization of MOGs materials as coreactants and opened a new horizon for development of novel ECL coreactants, holding promise for potential applications in various types of nucleic acid detection. Although we confirmed the capability of Ag-MOGs to detect DNA in buffer solution, developing more MOGs-composite materials and employing these materials for real clinical applications are also worthwhile consideration in future works.

Declaration of interests

The authors declare that they have no known competing financial interests or personal relationships that could have appeared to influence the work reported in this paper.

CRediT authorship contribution statement

Yang Li: Conceptualization, Methodology, Investigation, Validation, Writing - original draft, Data curation. **Li He:** Writing - review & editing. **Cheng Zhi Huang:** Formal analysis, Writing - review & editing. **Yuan Fang Li:** Funding acquisition, Formal analysis, Writing - review & editing, Project administration.

Acknowledgements

This study was supported by the National Natural Science Foundation of China (NSFC, No. 21575117).

Appendix A. Supplementary data

Supplementary data to this article can be found online at https://doi.org/10.1016/j.bios.2019.03.058.

References

Bai, J., Xi, B., Mao, H., Lin, Y., Ma, X., Feng, J., Xiong, S., 2018. One-step construction of N,P-codoped porous carbon sheets/CoP hybrids with enhanced lithium and potassium storage. Adv. Mater. 30 (35), 1802310.

Bairi, P., Roy, B., Nandi, A.K., 2011. pH and anion sensitive silver(i) coordinated melamine hydrogel with dye absorbing properties: metastability at low melamine concentration. J. Mater. Chem. 21 (32), 11747–11749.

Carrara, S., Arcudi, F., Prato, M., De Cola, L., 2017. Amine-rich nitrogen-doped carbon nanodots as a platform for self-enhancing electrochemiluminescence. Angew. Chem. 129 (17), 4835–4839.

Chen, Y., Xu, J., Su, J., Xiang, Y., Yuan, R., Chai, Y.Q., 2012. In situ hybridization chain reaction amplification for universal and highly sensitive electrochemiluminescent

detection of DNA. Anal. Chem. 84 (18), 7750–7755.
Dhara, B., Patra, P.P., Jha, P.K., Jadhav, S.V., Pavan Kumar, G.V., Ballav, N., 2014. Redox-induced photoluminescence of metal–organic coordination polymer gel. J. Phys. Chem. C 118 (33), 19287–19293.
Dong, Y.-P., Gao, T.-T., Zhou, Y., Jiang, L.-P., Zhu, J.-J., 2015. Anodic electrogenerated chemiluminescence of $Ru(bpy)_3^{2+}$ with CdSe quantum dots as coreactant and its application in quantitative detection of DNA. Sci. Rep. 5, 15392.
Fähnrich, K.A., Pravda, M., Guilbault, G.G., 2001. Recent applications of electrogenerated chemiluminescence in chemical analysis. Talanta 54 (4), 531–559.
Falcone, N., Kraatz, H.-B., 2018. Supramolecular assembly of peptide and metallopeptide gelators and their stimuli-responsive properties in biomedical applications. Chem. Eur J. 24 (54), 14316–14328.
Fei, J., Gao, L., Zhao, J., Du, C., Li, J., 2013. Responsive helical self-assembly of $AgNO_3$ and melamine through asymmetric coordination for Ag nanochain synthesis. Small 9 (7), 1021–1024.
Guo, W.L., Ding, H., Gu, C.Y., Liu, Y.H., Jiang, X.C., Su, B., Shao, Y.H., 2018. Potential-resolved multicolor electrochemiluminescence for multiplex immunoassay in a single sample. J. Am. Chem. Soc. 140 (46), 15904–15915.
Hu, L.Z., Xu, G.B., 2010. Applications and trends in electrochemiluminescence. Chem. Soc. Rev. 39 (8), 3275–3304.
Jayaramulu, K., Geyer, F., Petr, M., Zboril, R., Vollmer, D., Fischer, R.A., 2017. Shape controlled hierarchical porous hydrophobic/oleophilic metal-organic nanofibrous gel composites for oil adsorption. Adv. Mater. 29 (12), 1605307.
Jin, J., Takahashi, F., Kaneko, T., Nakamura, T., 2010. Characterization of electrochemiluminescence of tris(2,2′-bipyridine)ruthenium(II) with glyphosate as coreactant in aqueous solution. Electrochim. Acta 55 (20), 5532–5537.
Karan, C.K., Sau, M.C., Bhattacharjee, M., 2017. A copper(ii) metal–organic hydrogel as a multifunctional precatalyst for CuAAC reactions and chemical fixation of CO2 under solvent free conditions. Chem. Commun. 53 (9), 1526–1529.
Kitte, S.A., Wang, C., Li, S.P., Zholudov, Y., Qi, L.M., Li, J.P., Xu, G.B., 2016. Electrogenerated chemiluminescence of tris(2,2'-bipyridine)ruthenium(II) using N-(3-aminopropyl)diethanolamine as coreactant. Anal. Bioanal. Chem. 408 (25), 7059–7065.
Li, L., Liu, D., Mao, H., You, T., 2017. Multifunctional solid-state electrochemiluminescence sensing platform based on poly(ethylenimine) capped N-doped carbon dots as novel co-reactant. Biosens. Bioelectron. 89, 489–495.
Li, Y., Jiang, Z.W., Xiao, S.Y., Huang, C.Z., Li, Y.F., 2018. Terbium(III) organic gels: novel antenna effect-induced enhanced electrochemiluminescence emitters. Anal. Chem. 90 (20), 12191–12197.
Liu, X., Shi, L., Niu, W., Li, H., Xu, G., 2007a. Environmentally friendly and highly sensitive ruthenium(II) tris(2,2′-bipyridyl) electrochemiluminescent system using 2-(dibutylamino)ethanol as Co-reactant. Angew. Chem. Int. Ed. 46 (3), 421–424.
Liu, X.Q., Shi, L.H., Niu, W.X., Li, H.J., Xu, G.B., 2007b. Environmentally friendly and highly sensitive ruthenium(II) tris(2,2′-bipyridyl) electrochemiluminescent system using 2-(dibutylamino)ethanol as Co-reactant. Angew. Chem. Int. Ed. 46 (3), 421–424.
Liu, Z.Y., Qi, W.J., Xu, G.B., 2015. Recent advances in electrochemiluminescence. Chem. Soc. Rev. 44 (10), 3117–3142.
Long, Y.-M., Bao, L., Zhao, J.-Y., Zhang, Z.-L., Pang, D.-W., 2014. Revealing carbon nanodots as coreactants of the anodic electrochemiluminescence of $Ru(bpy)_3^{2+}$. Anal. Chem. 86 (15), 7224–7228.
Majumder, J., Dastidar, P., 2016. An easy access to organic salt-based stimuli-responsive and multifunctional supramolecular hydrogels. Chem. Eur J. 22 (27), 9267–9276.
Miao, W.J., 2008. Electrogenerated chemiluminescence and its biorelated applications. Chem. Rev. 108 (7), 2506–2553.
Miao, W.J., Choi, J.P., Bard, A.J., 2002. Electrogenerated chemiluminescence 69: the tris (2,2‘-bipyridine)ruthenium(II), $(Ru(bpy)_3^{2+})$/Tri-n-propylamine (TPrA) system RevisitedA new route involving TPrA•+ cation radicals. J. Am. Chem. Soc. 124 (48), 14478–14485.
Peng, Y.J., Li, Y., Li, L.L., Zhu, J.J., 2018. A label-free aptasensor for ultrasensitive Pb2+ detection based on electrochemiluminescence resonance energy transfer between carbon nitride nanofibers and $Ru(phen)_3^{2+}$. J. Hazard Mater. 359, 121–128.
Peng, Z.W., Yuan, D., Jiang, Z.W., Li, Y.F., 2017. Novel metal-organic gels of bis(benzimidazole)-based ligands with copper(II) for electrochemical selectively sensing of nitrite. Electrochim. Acta 238, 1–8.
Qi, B.-P., Zhang, X., Shang, B.-B., Xiang, D., Qu, W., Zhang, S., 2017a. A facile method to sensitively monitor chlorinated phenols based on Ru(bpy)32+ electrochemiluminescent system using graphene quantum dots as coreactants. Carbon 121, 72–78.
Qi, B.P., Zhang, X.R., Shang, B.B., Xiang, D.S., Qu, W.Y., Zhang, S.H., 2017b. A facile method to sensitively monitor chlorinated phenols based on $Ru(bpy)_3^{2+}$ electrochemiluminescent system using graphene quantum dots as coreactants. Carbon 121, 72–78.
Qi, Y., He, C.T., Lin, J.T., Lin, S.P., Liu, J., Huang, J.H., Xue, W., Yu, G.C., Chao, H.Y., Tong, Y.X., Qiao, Z.P., 2017c. Mild metal-organic-gel route for synthesis of stable sub-5-nm metal-organic framework nanocrystals. Nano Res. 10 (11), 3621–3628.
Qin, L., Wang, P., Guo, Y.W., Chen, C.Y., Liu, M.H., 2015. Self-assembled soft nanomaterials via silver(I)-Coordination: nanotube, nanofiber, and remarkably enhanced antibacterial effect. Adv. Sci. 2 (11), 1500134.
Richter, M.M., 2004. Electrochemiluminescence (ECL). Chem. Rev. 104 (6), 3003–3036.
Sentic, M., Milutinovic, M., Kanoufi, F., Manojlovic, D., Arbault, S., Sojic, N., 2014. Mapping electrogenerated chemiluminescence reactivity in space: mechanistic insight into model systems used in immunoassays. Chem. Sci. 5 (6), 2568–2572.
Shih, Y.-H., Chen, J.-H., Lin, Y., Chen, H.-T., Lin, C.-H., Huang, H.-Y., 2017. Nitrogen-doped porous carbon material derived from metal–organic gel for small biomolecular sensing. Chem. Commun. 53 (42), 5725–5728.
Sun, Y., Li, S., Zhou, Z.X., Saha, M.L., Datta, S., Zhang, M.M., Yan, X.Z., Tian, D.M., Wang, H., Wang, L., Li, X.P., Liu, M.H., Li, H., Stang, P.J., 2018. Alanine-based chiral metallogels via supramolecular coordination complex platforms: metallogelation induced chirality transfer. J. Am. Chem. Soc. 140 (9), 3257–3263.
Tang, L.Y., Liao, S.S., Qu, J.Q., 2018. Self-healing and multistimuli-responsive hydrogels formed via a cooperation strategy and their application in detecting biogenic amines. ACS Appl. Mater. Interfaces 10 (32), 27365–27373.
Thakur, N., Sharma, B., Bishnoi, S., Mishra, S.K., Nayak, D., Kumar, A., Sarma, T.K., 2018. Multifunctional inosine monophosphate coordinated metal–organic hydrogel: multistimuli responsiveness, self-healing properties, and separation of water from organic solvents. ACS Sustain. Chem. Eng. 6 (7), 8659–8671.
Tu, T., Assenmacher, W., Peterlik, H., Weisbarth, R., Nieger, M., Dötz, K.H., 2007. An air-stable organometallic low-molecular-mass gelator: synthesis, aggregation, and catalytic application of a palladium pincer complex. Angew. Chem. Int. Ed. 46 (33), 6368–6371.
Valenti, G., Rampazzo, E., Bonacchi, S., Petrizza, L., Marcaccio, M., Montalti, M., Prodi, L., Paolucci, F., 2016. Variable doping induces mechanism swapping in electrogenerated chemiluminescence of $Ru(bpy)_3^{2+}$ core–shell silica nanoparticles. J. Am. Chem. Soc. 138 (49), 15935–15942.
Vallejo-Sánchez, D., Amo-Ochoa, P., Beobide, G., Castillo, O., Fröba, M., Hoffmann, F., Luque, A., Ocón, P., Pérez-Yáñez, S., 2017. Chemically resistant, shapeable, and conducting metal-organic gels and aerogels built from dithiooxamidato ligand. Adv. Funct. Mater. 27 (15), 1605448.
Wang, X.F., Gao, H.F., Qi, H.L., Gao, Q., Zhang, C.X., 2018. Proximity hybridization-regulated immunoassay for cell surface protein and protein-overexpressing cancer cells via electrochemiluminescence. Anal. Chem. 90 (5), 3013–3018.
Wu, S.Z., Zhou, Z.Y., Xu, L.R., Su, B., Fang, Q., 2014. Integrating bipolar electrochemistry and electrochemiluminescence imaging with microdroplets for chemical analysis. Biosens. Bioelectron. 53, 148–153.
Xing, H., Zhai, Q., Zhang, X., Li, J., Wang, E., 2018a. Boron nitride quantum dots as efficient coreactant for enhanced electrochemiluminescence of ruthenium(II) tris (2,2′-bipyridyl). Anal. Chem. 90 (3), 2141–2147.
Xing, H.H., Zhai, Q.F., Zhang, X.W., Li, J., Wang, E.K., 2018b. Boron nitride quantum dots as efficient coreactant for enhanced electrochemiluminescence of ruthenium(II) tris (2,2′-bipyridyl). Anal. Chem. 90 (3), 2141–2147.
Zhang, J.Y., Su, C.Y., 2013. Metal-organic gels: from discrete metallogelators to coordination polymers. Coord. Chem. Rev. 257 (7), 1373–1408.